Dynamic Performance Analysis of Deep Bars Squirrel Cage Induction Motor by Simulation

Mihai Iordache*, Lucia Dumitriu*, Dragos Niculae*, Neculai Galan*, Sorin Deleanu† and Lucian Mandache**
* "Politehnica" University of Bucharest, Romania, mihai.iordache@upb.ro, lucia.dumitriu@upb.ro, dragos.niculae@upb.ro, galannicolae@yahoo.com
† Northern Alberta Institute of Technology, Edmonton, Canada, sorind@nait.ca
** University of Craiova, Faculty of Electrical Engineering, Craiova, Romania, lmandache@elth.ucv.ro

Abstract - **The rotor parameters of the squirrel cage induction machine, resistance and leakage inductance, depend upon the frequency of the rotor circuit, mostly due to the skin effect. For low values of the rotor frequency (less than 10 - 15 Hz), corresponding to the quasi-linear branch of the torque-speed curve between synchronous speed and the critical one, the skin effect is quite insignificant. However, for higher frequencies (e.g. 50Hz and/or 60Hz, at starting), this variation of the parameters cannot be neglected. In this paper, the analytic relationships developed for expressing the rotor resistance and leakage inductance as functions of slip/frequency, directly result from the skin effect theory. The induction motor model based upon Park-Blondel equations have been used to analyze its dynamic (transient) behavior. Park-Blondel equations are nonlinear, because of their intrinsic structure, the rotor parameters variation with the frequency, saturation of the magnetic core, and the dependency of the load torque with respect to the rotor angular frequency. For solving the induction motor system of equations, the authors used MATLAB software package due to its enhanced capabilities in terms of integrating ordinary differential equations. When analyzing the induction motor operating at steady state, we used the well-known Ő (Steinmetz) per-phase equivalent circuit. Although, the magnetizing inductance is considered as the current-controlled nonlinear inductor while the rotor resistor as a time-variable resistor. For steady-state analysis, both ENCAP (Electrical Nonlinear Circuit Analysis) and SPICE software packages have been used in order to be able to assess the results. In both cases, the induction motor model is derived from modified nodal equations. This gives the possibility to apply Fourier analysis for all current and voltage waveforms and compute any high order harmonics. Following the computing of harmonic content, we assessed the steady state characteristics (power factor, efficiency, etc.) of the induction motor, while the equivalent circuit parameters determined through calculations closely match the parameter values obtained from the catalogue data.**

Keywords - *induction motor, state equations, transient behavior, deep rotor bars, saturation phenomena, stead-steady behavior, skin effect*

I. INTRODUCTION

In many studies regarding the estimation the induction machine parameters, the authors included the skin effect and the saturation of the magnetic circuit [1-9, 12-14]. When considering applications of electric AC drives using three-phase induction motors with deep bars in the rotor circuit, both mathematical model of the induction motor and the overall control strategy have been modified in order to maximize the performance [6]. Most of the vector drives use to rotor flux control due to the simplicity of the mathematical model which demands less "real-time" computation.

However, for the motor with deep rotor bars, the rotor flux significantly varies inside the rotor magnetic core, so cannot be precisely defined. As a result, the drive control using the air gap flux appears as an attractive alternative. However, when using the pseudo rotor flux, one can achieve similar performances to the rotor flux orientation case, when considering the equivalent rotor parameters. The squirrel cage with deep rotor bars can be made equivalent with a two rotor cages, one of these described by constant parameters [8].

The induction motor with deep bars is described by a mathematical model which includes the skin effect upon the rotor parameters and the saturation of the magnetic circuit as well and enables the simulation of various operating modes. The frequency of the stator winding is constant and equal to the power supply frequency, resulting constant stator parameters. The rotor parameters are assumed constant, independent of the rotor current frequency when this one has low values (0 to 10…15 Hz, the latter one usually being associated with the critical slip/speed). However, for higher values of the rotor current frequency, the rotor resistance and leakage inductance depend upon the frequency (slip) through relationships developed from the skin effect theory.

In addition to the skin effect, the saturation of the magnetic circuit comes into effect when the magnetizing inductivity L_m varies. In Fig. 1, L_m appears variable in time. In fact, this curve explains the magnetic circuit saturation effect during the start-up process, when the induction motor has deep bars. In order to approach real starting condition, a load torque M_r, variable with the speed was proposed in Fig. 2.

The induction motor analysis for steady-state analysis purpose requires the state equations referred to the "*d*, *q*, 0" system of coordinates, in which the time derivatives are made equal to zero, excepting the mechanical equation. Once integrated over a long time span, the mechanical equation can deliver the steady state value of rotor mechanical speed and consequently, the stator and rotor currents, electromagnetic torque, etc.

Other methods for obtaining the steady state characteristics are based upon the solving of the induction motor equivalent circuit (see Fig. 3) or by applying the state equations and / or the modified nodal equations.

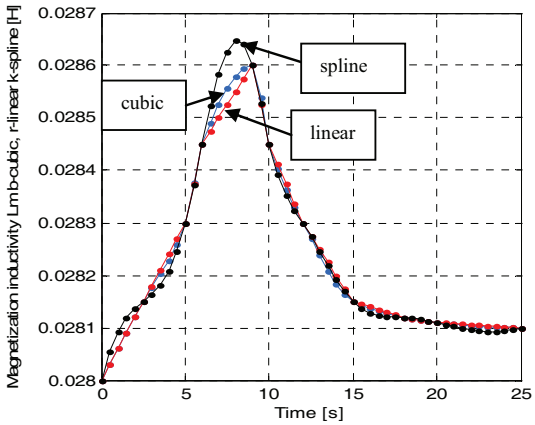

Fig. 1. The magnetization inductivity variation versus time.

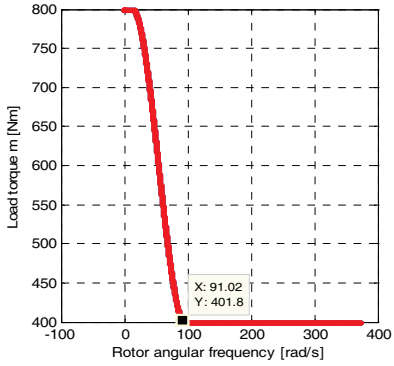

Fig. 2. The load torque variation versus rotor angular frequency.

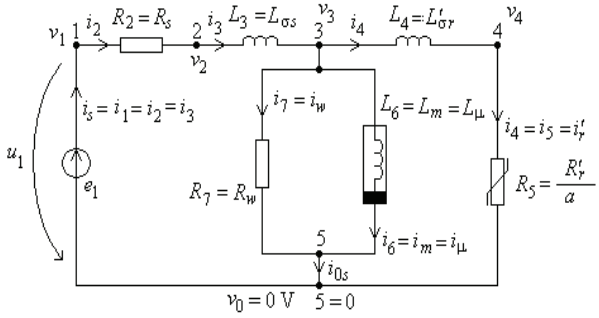

Fig. 3. Induction motor equivalent circuit.

The latter one (called the *brute force*) involves a number of iterations until the steady state solutions is obtained, through a process which must satisfy an imposed convergence criterion [10, 11, 14].

The first major outcome of this paper was to analyze the deep bars induction motor steady state behavior and characteristics for non-saturated magnetic circuit versus the situation when we assumed the magnetic circuit saturated (see the $\prod$ equivalent circuit of the induction motor shown in Fig. 3). When the magnetic circuit saturation was included, the magnetization inductor $L_6 = L_m$ was modeled as a current-controlled nonlinear inductor with its magnetic flux depending upon the magnetizing current $\varphi = \hat{\varphi}(i_m)$. However, in this paper, the steady state study follows the transient study as particular regime.

The second major outcome of this paper was to analyze the transient behavior of the deep bars induction motor, using the state equations and/or the modified nodal equations in the time domain (the semi-state equations), based on the brute force method. For transient purposes, the rotor resistor R'_r/a (a – being the slip) was modeled as a time-variable (parametric) function, in which the slip was calculated at each time step.

The simulations were performed by using the SPICE and/or the ENCAP – Electrical Nonlinear Circuit Analysis software packages [10, 11]. When using these packages, the deep bars induction motor model was constructed in terms of the modified nodal equations, being very appropriate for the Fourier analysis for all current and voltage waveforms. In this way we could compute any high order voltage/current harmonics, following the determination of the time dependency of such quantities. The voltage/current harmonic calculation represents the input towards the deep bars induction motor performances assessment (e.g. more harmonic content means less efficiency, poor power factor, etc.).

In addition to the performances, some adjacent effects like the electromagnetic forces and the parasitic torques can be analytically approximated from voltage/current harmonics [15].

II. Simulation of the Induction Motor for Transient Conditions

The induction motor transient analysis was performed starting with the dynamic state equations expressed in the d, q, 0 reference frame and the rotor quantities referred to the stator [7]:

$$\frac{d\varphi_{sd}}{dt} = -R_s\left(\frac{1}{\sigma L_s}\left(\varphi_{sd} - \frac{L_m}{L'_r}\varphi'_{rd}\right)\right) + \omega_1\varphi_{sq} + u_{sd} \quad (1,a)$$

$$\frac{d\varphi_{sq}}{dt} = -R_s\left(\frac{1}{\sigma L_s}\left(\varphi_{sq} - \frac{L_m}{L'_r}\varphi'_{rq}\right)\right) - \omega_1\varphi_{sd} + u_{sq} \quad (1,b)$$

$$\frac{d\varphi'_{rd}}{dt} = -R'_r\left(\frac{1}{\sigma L'_r}\left(\varphi'_{rd} - \frac{L_m}{L_s}\varphi_{sd}\right)\right) + (\omega_1 - \omega)\varphi'_{rq} \quad (1,c)$$

$$\frac{d\varphi'_{rq}}{dt} = -R'_r\left(\frac{1}{\sigma L'_r}\left(\varphi'_{rq} - \frac{L_m}{L_s}\varphi_{sq}\right)\right) - (\omega_1 - \omega)\varphi'_{ra} \quad (1,d)$$

$$\frac{d\omega}{dt} = \frac{3p^2}{2J}\left(\varphi_{sd}\frac{1}{\sigma L_s}\left(\varphi_{sq} - \frac{L_m}{L'_r}\varphi'_{rq}\right) - \varphi_{sq}\frac{1}{\sigma L_s}\left(\varphi_{sd} - \frac{L_m}{L'_r}\varphi'_{rd}\right)\right) - \frac{pM_r}{J} \quad (1,e)$$

$$\frac{d\theta}{dt} = \omega \quad (1,f)$$

where: φ_{sd} - is the stator magnetic flux axis in the direction of "d-axis", φ_{sq} - represents the stator magnetic flux in the direction of "q-axis" (quadrature), φ'_{rd} - is the rotor magnetic flux along the "d-axis", φ'_{rq} - represents the

rotor magnetic flux with respect to the "q-axis", ω – is the rotor angular frequency ($\omega = p\Omega$, p – number of the pole pairs and Ω is the mechanical angular speed), $\omega_r = \omega_1 - \omega$ - is the rotor current angular frequency, ω_1 - represents the stator angular frequency and θ - is the electric angle which gives the rotor position in respect of the stator (see Fig. 4, θ is the angle between the FS axis and FR axis). In the majority of the models FS designates the magnetic axis of stator "phase A" winding while the FR stays for the rotor "phase a" winding.

The state vector has the following expression:

$$\boldsymbol{x} = \left[\varphi_{sd}, \varphi_{sq}, \varphi'_{rd}, \varphi'_{rq}, \omega, \theta\right]^{t}. \tag{2}$$

The stator and the rotor magnetic fluxes can be expresses as functions of the currents and inductances as following:

$$\begin{aligned} \varphi_{sd} &= L_s i_{sd} + L_m i'_{rd}; \qquad \varphi_{sq} = L_s i_{sq} + L_m i'_{rq}; \\ \varphi'_{rd} &= L'_r i'_{rd} + L_m i_{sd}; \qquad \varphi'_{rq} = L'_r i'_{rq} + L_m i_{sq}. \end{aligned} \tag{3}$$

When solving the equations (3) for the currents i_{sd}, i_{sq}, i'_{rd} and i'_{rq} we obtained:

$$\begin{aligned} i_{sd} &= \frac{1}{\sigma L_s}\left(\varphi_{sd} - \frac{L_m}{L'_r}\varphi'_{rd}\right), i_{sq} = \frac{1}{\sigma L_s}\left(\varphi_{sq} - \frac{L_m}{L'_r}\varphi'_{rq}\right), \\ i'_{rd} &= \frac{1}{\sigma L'_r}\left(\varphi'_{rd} - \frac{L_m}{L_s}\varphi_{sd}\right), i'_{rq} = \frac{1}{\sigma L'_r}\left(\varphi'_{rq} - \frac{L_m}{L_s}\varphi_{sq}\right). \end{aligned} \tag{4}$$

In the relations (1) – (4) have been used the: $u_{sd} = \sqrt{2}U_1$; $u_{sq} = 0.0$; R_s – is the stator resistance; R'_r – represents the rotor resistance referred to the stator; L_s – is the cyclical stator inductance, defined as the sum of the stator leakage inductance $L_{s\sigma}$ and the useful cyclical stator inductance L_{11}; L'_r – represents the cyclical rotor inductance, defined as the sum between the rotor leakage inductance $L'_{r\sigma}$ and the useful cyclical inductance L'_{22} - all of the rotor inductances are referred to the stator; L_m – is the cyclical mutual inductivity between the stator and the rotor, given by the relationship $L_m = 3M_m/2$, in which M_m is the maximum value of the mutual inductivity, measured between one stator phase winding and one rotor phase winding having the same direction; ω_1 - represents the stator angular frequency; ω - is the mechanical angular frequency (at the motor shaft); $\Omega_1 = \omega_1 / p$ - represents the angular speed of the revolving electromagnetic field with respect of the stator (synchronous speed); $\Omega = \omega / p$ - is the mechanical angular speed of the rotor; p – the number of the pole pairs; J – the rotor moment of inertia and M_r – is the load torque. The non-dimensional "leakage coefficient" σ has the expression:

$$\sigma = 1 - \frac{L_m^2}{L_s L'_r}. \tag{5}$$

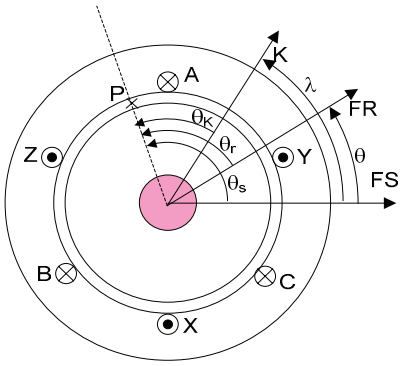

Fig. 4. Structure of the reference systems.

The electromagnetic torque can be calculated starting from the definition and using (4):

$$\begin{aligned} M &= \frac{3p}{2}\left(\varphi_{sd} i_{sq} - \varphi_{sq} i_{sd}\right) = \\ &= \frac{3p}{2}\left(\varphi_{sd} \cdot \frac{1}{\sigma L_s}\left(\varphi_{sq} - \frac{L_m}{L'_r}\varphi'_{rq}\right) - \right. \\ &\left. - \varphi_{sq} \cdot \frac{1}{\sigma L_s}\left(\varphi_{sd} - \frac{L_m}{L'_r}\varphi'_{rd}\right)\right) \end{aligned} \tag{6}$$

or:

$$\begin{aligned} M &= \frac{3p}{2}\left(\varphi'_{rd} i'_{rq} - \varphi'_{rq} i'_{rd}\right) = \\ &= \frac{3p}{2}\left(\varphi'_{rd} \frac{1}{\sigma L'_r}\left(\varphi'_{rq} - \frac{L_m}{L_s}\varphi_{sq}\right) - \right. \\ &\left. - \varphi'_{rq} \cdot \frac{1}{\sigma L'_r}\left(\varphi'_{rd} - \frac{L_m}{L_s}\varphi_{sd}\right)\right). \end{aligned} \tag{7}$$

The stator and rotor phase currents i_A, i_B, i_C respectively i'_a, i'_b, i'_c can by expressed, as function of the d, q, 0 stator and rotor currents following a transformation of coordinates [7]:

$$\begin{aligned} i_A(t) &= i_{ds}(t)\cdot\cos(\omega_1 t) - i_{qs}(t)\cdot\sin(\omega_1 t) + i_{0s}; \\ i_B(t) &= i_{ds}(t)\cdot\cos\left(\omega_1 t - \frac{2\pi}{3}\right) - i_{qs}(t)\cdot\sin\left(\omega_1 t - \frac{2\pi}{3}\right) + i_{0s}; \\ i_C(t) &= i_{ds}(t)\cdot\cos\left(\omega_1 t + \frac{2\pi}{3}\right) - i_{qs}(t)\cdot\sin\left(\omega_1 t + \frac{2\pi}{3}\right) + i_{0s}; \\ i'_a(t) &= i'_{dr}(t)\cdot\cos\left((\omega_1 - \omega)t\right) - i'_{qr}(t)\cdot\sin\left((\omega_1 - \omega)t\right) + i_{0r}; \\ i'_b(t) &= i'_{dr}(t)\cdot\cos\left((\omega_1 - \omega)t - \frac{2\pi}{3}\right) - i'_{qr}(t)\cdot\sin\left((\omega_1 - \omega)t - \frac{2\pi}{3}\right) + i_{0r}; \\ i'_c(t) &= i'_{dr}(t)\cdot\cos\left((\omega_1 - \omega)t + \frac{2\pi}{3}\right) - i'_{qr}(t)\cdot\sin\left((\omega_1 - \omega)t + \frac{2\pi}{3}\right) + i_{0r} \end{aligned} \tag{8}$$

Assuming the induction motor with identical phase windings characteristics, operating under balanced conditions, the stator and the rotor zero-sequence currents will not be present $i_{0s} = 0$, respectively $i_{0r} = 0$.

The skin effect analysis shows that the rotor resistance R'_r referred at the stator increases with $\sqrt{\omega_r}$, while the

leakage inductance $L'_{r\sigma}$ decreases with $\sqrt{\omega_r}$, where ω_r is the rotor angular frequency. Therefore, the rotor parameters referred to the stator can be expressed as following [7]:

$$\begin{aligned} &R'_r(\omega_r) = R'_r = ct. \quad \text{for } \omega_r \in (0, \omega_{rx}); \\ &R'_r(\omega_r) = k_1 + k_2\sqrt{\omega_r}; \ \omega_r > \omega_{rx}; \\ &L'_r(\omega_r) = L'_r = ct. \quad \text{for } \omega_r \in (0, \omega_{rx}); \\ &L'_r(\omega_r) = L_m + k_3 - \frac{k_4}{\sqrt{\omega_r}}; \ \omega_r > \omega_{rx}. \end{aligned} \tag{9}$$

The constants k_1, k_2, k_3 and k_4 are determined from the continuity condition at the point $\omega_r = \omega_{rx}$ (ω_{rx} represents the value of the angular frequency associated with the critical slip), while the values of the electrical parameters for the squirrel cage at starting point (slip value $a = 1$), can be extracted from the available catalogue data for an induction motor.

Typically for the range $\omega_r < \omega_{rx}$, the rotor parameters are considered constant, while for $\omega_r \geq \omega_{rx}$ the rotor parameters vary with the rotor angular frequency ω_r according to relations (9). These are valid for a wide range of frequencies from rotor circuit.

As example, we consider an induction motor for designated for traction purposes (MABT-2). This induction motor has the following ratings:

$P_n = 100$ kW; $U_n = 560$ V; $U_{fn} = 323.32$ V; $I_{fn} = I_n = 130$ A; $n_1 = 1200$ rpm, $n = 1168.8$ rpm - n_1 (n) is the synchronous revolving speed; $Z_b = Z_n = U_{fn}/I_{fn} = 2.48\ \Omega$; $f_n = f_1 = 60$ Hz; $p = 3$; $R_s = 0.053\ \Omega$; $R'_r = 0.0657\ \Omega$; $L_{s\sigma} = 1.034$ mH; $L'_{r\sigma} = 0.955$ mH; $L_m = 28.1$ mH; $\eta = 0.897$ %; $\cos\varphi_{1n} = 0.87$; $J = 3.38$ kgm^2 or $J = 60.0$ kgm^2; $i_p = \frac{I_{fp}}{I_{fn}} = 4$; $m_p = \frac{M_p}{M_n} = 1.1$; $m_m = \frac{M_m}{M_n} = 1.8$. Stator windings have a Y-connection.

With the values from above, the next quantities are calculated: $M_n = 817$ Nm; $M_p = 898.7$ Nm; $I_p = 520$ A; $S_n = 128094.8$ VA; $a_n = 0.026$; $P_{1n} = S_n \bullet \cos\varphi_{1n} = 111442.5$ W.

From [7], if $\omega_{rx} = 81$ rad/s, when introducing the data from above in the relationships (9), the numerical values for the rotor electrical parameters referred to the stator can be described as:

$$\begin{aligned} &L'_r(\omega_r) = 0{,}0281 + \begin{cases} 0{,}000955\,H; & \omega_r \in [0; 81] \\ 0{,}000155 + 0{,}0072\dfrac{1}{\sqrt{\omega_r}}; & 81 < \omega_r \leq \omega_1 \end{cases} \\ &R'_r(\omega_r) = \begin{cases} 0{,}065434; & \omega_r \in [0; 81] \\ 0.000904 + 0{,}00717\sqrt{\omega_r}; & 81 < \omega_r \leq \omega_1 \end{cases} \\ &\text{with} \quad \omega_1 = 120\pi \end{aligned} \tag{10}$$

A complete procedure for determining the transient behavior at starting of the squirrel cage induction motor with deep bars consists of the following steps:

• In the dynamic state equations (1), the rotor electrical parameters are introduced using the relationships (10), which in fact consider the skin effect.

• The influence of the magnetic circuit saturation is revealed by the dependency of the magnetic inductance with the time given in Fig. 1.

The load torque encountered by the induction motor at the shaft has a time dependency given in Fig. 2.

Following the application of some ordinary integration routines (available in MATLAB programming environment) to solve the equations (1), we've obtained the results summarized in Fig. 5 – 18.

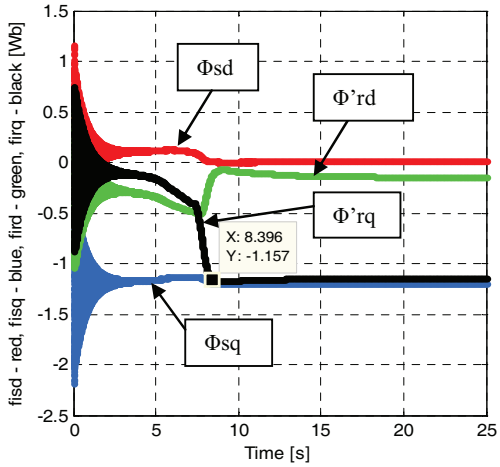

Fig. 5. The stator and rotor magnetic fluxes in the d, q, 0 reference frame as functions of time.

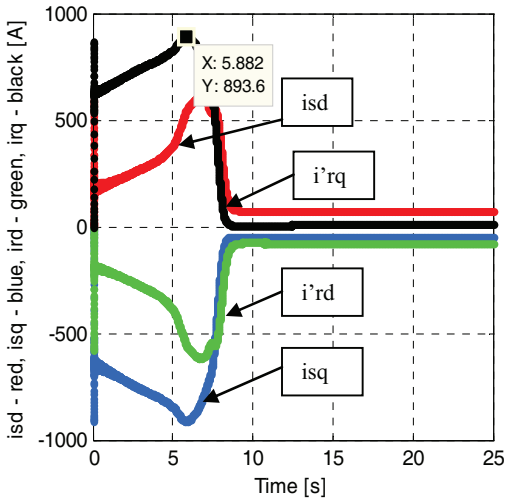

Fig. 6. The stator and rotor currents in the d, q, 0 reference frame as functions of time.

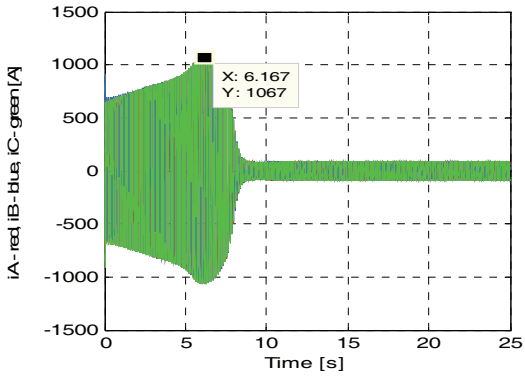

Fig. 7. The stator currents as functions of time.

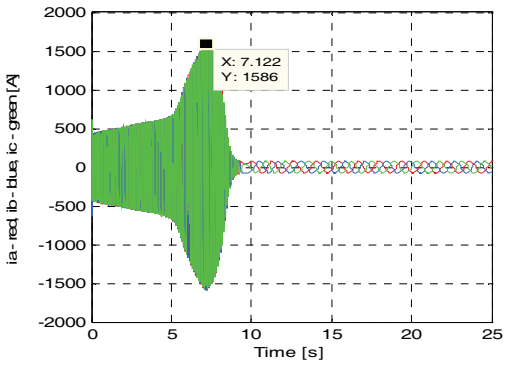

Fig. 8. The rotor currents as functions of time.

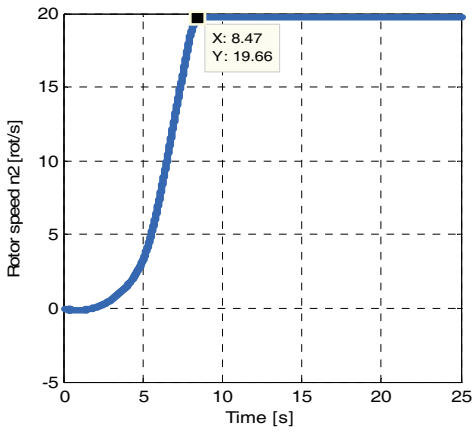

Fig. 9. The revolving speed at the shaft as function of time.

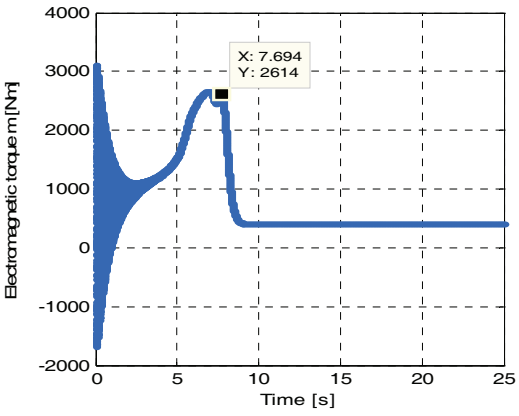

Fig. 10. The electromagnetic torque vs. time.

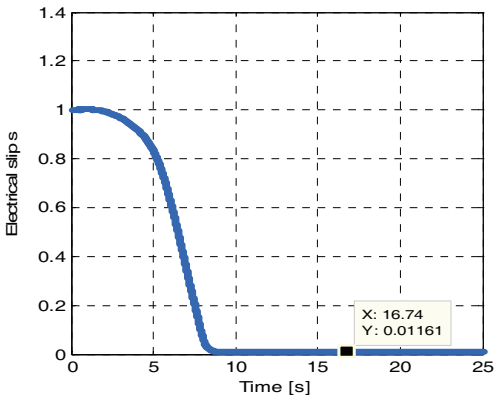

Fig. 11. The slip $s = a$ as function of time.

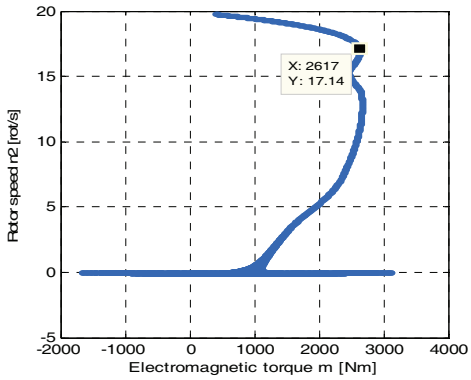

Fig. 12. The slip $s = a$ as function of time Mechanical characteristic: the rotor speed as function of the electromagnetic (developed) torque.

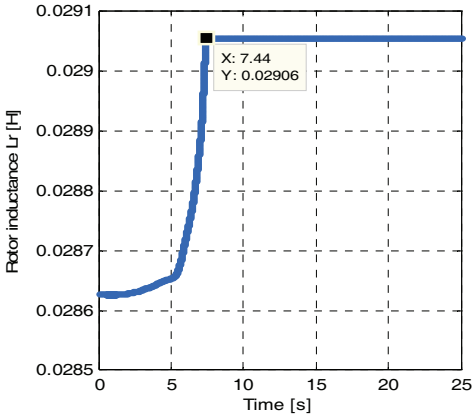

Fig. 13. The rotor inductance vs. time.

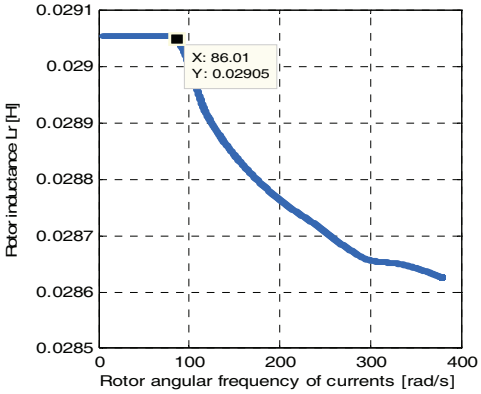

Fig. 14. The rotor inductance vs. rotor angular frequency.

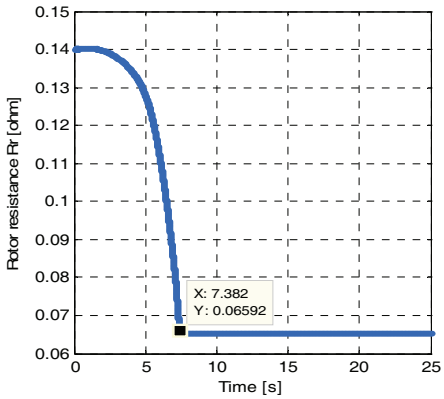

Fig. 15. The rotor resistance vs. time.

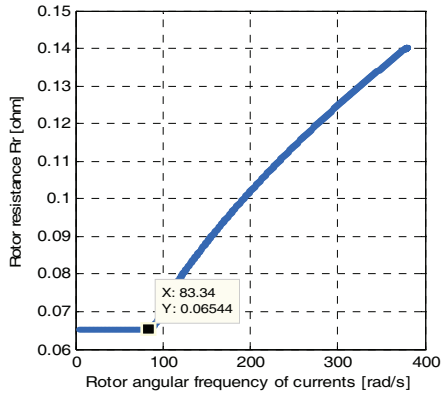

Fig. 16. The rotor resistance vs. angular frequency of the rotor circuit.

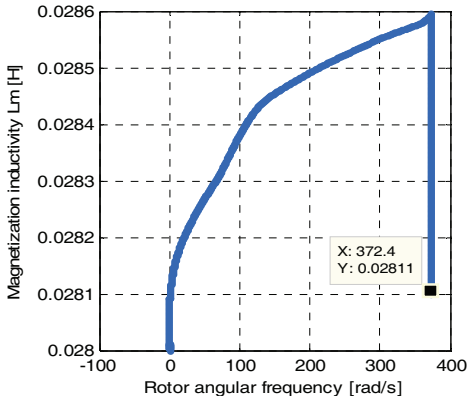

Fig. 17. The magnetization inductivity (inductance) vs. time.

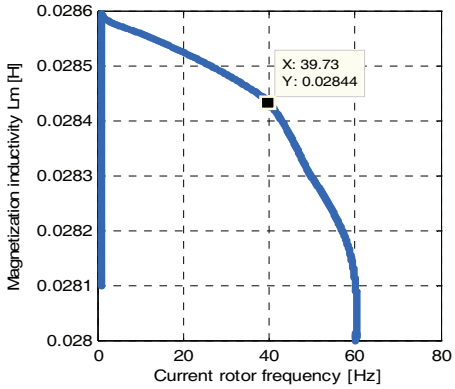

Fig. 18. The magnetization inductivity vs. rotor circuit frequency.

The synchronous reference frame is the most appropriate for the description of the current transients. In the first few cycles, for constant values of the rotor parameters, the rotor angular speed is low. For these conditions, only the transformer action of the induction machine will contribute in terms of the back EMF e_t, while the back EMF component due to the motion e_m is negligible. The zero-crossing of e_t is associated with the maximum values of the magnetic flux of the phase the e_t was accounted for (the mathematical linkage between e_t and the magnetic flux is given by the Faraday-Lenz law [7]). The phase voltage has a relatively low value at this moment. However, due to the lack of back EMF, the phase impedance which limits the current consists of a series circuit of the winding resistance and leakage reactance. This explains why the starting current can reach several times the value of the nominal current. In a phase winding, the current value at the first instant of the starting process, strongly depends upon the instantaneous value of the applied voltage in that particular phase. The closer to zero the transformation back EMF e_t is at the first instant, the higher the phase current is recorded for that phase.

Once the starting process being initiated, the induction motor accelerates the revolving speed at the shaft increases and the motion back EMF component e_m increases as well, limiting the value of the current. The transformation back EMF e_t becomes way less significant, while the motor approaches the steady state. When considering the rotor parameters depending upon the angular frequency of the rotor circuit, we recorder a longer starting process, followed by a steady state operation highlighted by the sinusoidal stator current waveforms of at the nominal frequency (see Fig. 8). For a given value of the applied voltage, the magnitude of the stator winding currents (and of the rotor currents as well!) depends upon the load torque and the presence of the motion back EMF. The revolving magnetic field originated by the stator winding, will induce back EMF in the short circuited rotor windings. Consequently, the currents which will be established in the rotor windings will oppose to the variation of the stator currents (Lenz's law). This explains the fact that the absolute value of the magnetizing current is always less than each of the stator and/or rotor currents absolute values. When operating in steady state conditions, the magnitude of the stator current is directly related to the shaft torque. If the torque demand decreases, the input current decreases and so does the voltage drop across the stator winding impedance. If the applied voltage is rigorously constant, the magnetizing current value will slightly increase due to higher voltage at the terminals of the branch containing the magnetizing impedance (see Fig. 3 for the equivalent circuit configuration). The rotor current variation is following the shaft torque variation with a delay conditioned by the value of the rotor circuit time constant.

In our application, initially the induction motor operates at steady state, with a well determined slip value. When the load demand decreases, the revolving speed of the rotor increases surpassing the value where the developed torque equals the load torque. The motor slip significantly decays following a complex time function. The currents are described by periodical functions of a certain frequency, which has a lower value than the frequency corresponding to the new torque "equilibrium" point. In our application, this part of the transient process is occurring when $t \in (6.167; 8.4)$. Following this slice of overall transient process, a new stable operating point is established for lower slip value due to the lower torque demand (see Figs. 7, 8 and 10).

In fig. 10 we observe a time variation of the electromagnetic torque which is quite characteristic for the starting process, yet longer due to the variable rotor parameters. When analyzing the speed-torque characteristic for the induction machine with frequency dependent rotor parameters (the skin effect was included), one can figure out that the starting torque is larger than the rated: the induction motor can successfully start under rated torque conditions. For the electromagnetic torque – time curve from fig. 10, we assumed that the rotor parameters depend upon the frequency of the rotor currents. There are two separate branches on the electromagnetic torque – time curve:

Zone 1 where the rotor parameters are variable, the torque slip dependency is not covered by Kloss relation-

ship and the starting torque comes with a much higher value in comparison with the constant rotor parameters case;

Zone 2 where the rotor parameters are constant, including the breakdown (maximum) torque value;

However, for the deep bar squirrel cage induction motor, the maximum torque has a lower value comparing to other induction motor types: this fact is motivated by a larger value of the rotor leakage reactance.

III. Simulation of the Induction Motor Operating in State-Steady Conditions

Let's consider the $\prod$ (Steinmetz) equivalent circuit of the induction motor shown in Fig. 3, which contains a current-controlled (c.c.) nonlinear inductor L6 with the nonlinear characteristic $\varphi_{L6} = \hat{\varphi}_{L6}(i_6)$ and a time-variable resistor $R_5 = \dfrac{R'_r}{a} = f(t)$, a being the slip.

The state equations in symbolic–normal form have been expressed as:

$$\frac{\mathrm{d}}{\mathrm{d}t}\begin{bmatrix} i_3 \\ i_4 \\ i_6 \end{bmatrix} = \begin{bmatrix} -\dfrac{R_2+R_7}{L_3} & \dfrac{R_7}{L_2} & \dfrac{R_7}{L_2} \\ \dfrac{R_7}{L_4} & -\dfrac{R_7+R_{p5}}{L_4} & -\dfrac{R_7}{L_4} \\ \dfrac{R_7}{L_{di6}(i_6)} & -\dfrac{R_7}{L_{di6}(i_6)} & -\dfrac{R_7}{L_{di6}(i_6)} \end{bmatrix} \cdot \begin{bmatrix} i_3 \\ i_4 \\ i_6 \end{bmatrix} + \begin{bmatrix} \dfrac{1}{L_3} \\ 0 \\ 0 \end{bmatrix} \cdot [e_1] \tag{11}$$

with the differential inductance $L_{di6}(i_6) = \dfrac{\partial \varphi_{L6}}{\partial i_6}$.

To integrate the state equations (11) we can use any integration routine available with MATLAB software package. The modified nodal equations, corresponding to the implicit integration Euler algorithm are:

$$\begin{aligned}
&(n_1):\ G_2 v_{1,j+1}^{(k+1)} - G_2 v_{2,j+1}^{(k+1)} - i_{1,j+1}^{(k+1)} = 0,\\
&(n_2):\ -G_2 v_{1,j+1}^{(k+1)} + \left(G_2 + \frac{h}{L_3}\right) v_{2,j+1}^{(k+1)} - \frac{h}{L_3} v_{3,j+1}^{(k+1)} = -i_{3,j},\\
&(n_3):\ -\frac{h}{L_3} v_{2,j+1}^{(k+1)} + \left(\frac{h}{L_3} + \frac{h}{L_4} + G_7\right) v_{3,j+1}^{(k+1)} - \frac{h}{L_4} v_{4,j+1}^{(k+1)} + \\
&\qquad + i_{6,j+1}^{(k+1)} = i_{3,j} - i_{4,j},\\
&(n_4):\ -\frac{h}{L_4} v_{3j+1}^{(k+1)} + \left(\frac{h}{L_4} + G_{p5}\right) v_{4,j+1}^{(k+1)} = i_{4,j},\\
&(b_1):\ -v_{1,j+1}^{(k+1)} = -e_{1,(j+1)},\\
&(b_6):\ v_{3,j+1}^{(k+1)} - \frac{L_{di6}\left(s_{j+1}^{(k)}\right)}{h} i_{6,j+1}^{(k+1)} = \frac{\Phi_{L6}\left(s_{j+1}^{(k)}\right)}{h} - \\
&\qquad - \frac{L_{di6}\left(s_j\right)}{h} \cdot i_{6,j} - \frac{\Phi_{L6,j}}{h},
\end{aligned} \tag{12}$$

where the independent variable vector, at the time moment $t_{j+1} = t_j + h$ and at the $(k+1)^{\text{th}}$, iteration has the following structure:

$$\boldsymbol{x}_{j+1}^{(k+1)} = \left[v_{1,j+1}^{(k+1)}\ v_{2,j+1}^{(k+1)}\ v_{3,j+1}^{(k+1)}\ v_{4,j+1}^{(k+1)}\ i_{1,j+1}^{(k+1)}\ i_{6,j+1}^{(k+1)}\right]^{\mathrm{t}} \tag{13}$$

The magnetization characteristic $\varphi_{L6} = \hat{\varphi}_{L6}(i_6)$, at the time moment $t_{j+1} = t_j + h$ and at the $(k+1)^{\text{th}}$ iteration, is piecewise linear approximated by the relation:

$$\varphi_{L6,j+1}^{(k+1)} = L_{di6}\left(s_{j+1}^{(k)}\right) \cdot i_{6,j+1}^{(k+1)} + \Phi_{L6}\left(s_{j+1}^{(k)}\right) \tag{14}$$

In the relation (14) $s_{j+1}^{(k)}$ is the segment at the time moment $t_{j+1} = t_j + h$ and at the $(k)^{\text{th}}$ iteration.

Both programs SPICE and ENCAP are based upon the modified nodal equations (12), but while SPICE uses the trapezoidal integration algorithm, ENCAP uses the implicit integration Euler algorithm.

To solve the nonlinear algebraic equations at each time step, both programs use the Newton-Raphson algorithm, [1-7].

IV. Results Obtained by Simulations

The magnetization nonlinear characteristic $\varphi_{L6} = \hat{\varphi}_{L6}(i_6)$ was derived from points determined experimentally (Fig. 19).

The characteristic of the time-variable resistor R5 is also given by points as function of time. When running the simulation using the ENCAP program, the authors obtained the results shown in Fig. 19 – 25.

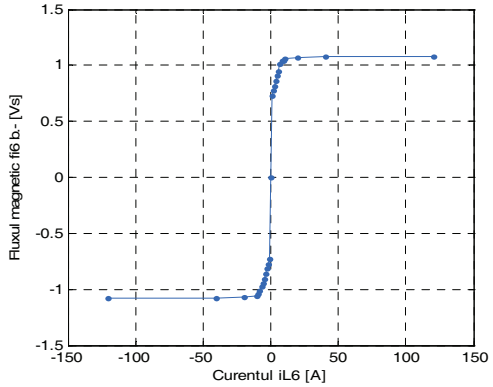

Fig. 19. Magnetization nonlinear characteristic $\varphi_{L6} = \hat{\varphi}_{L6}(i_6)$.

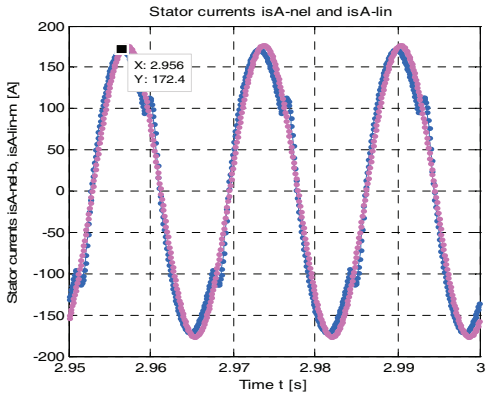

Fig. 20. Stator current i_{sA} vs time, magenta – linear case, blue – nonlinear case

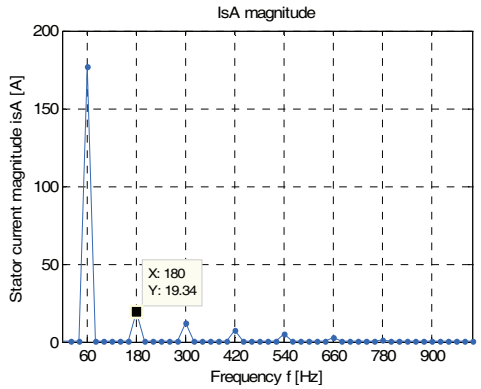

Fig. 21. Stator current magnitude I_{sA} vs. frequency.

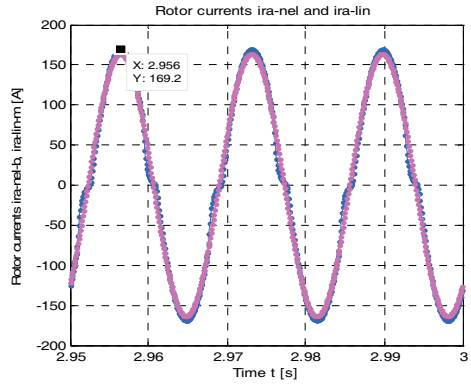

Fig. 22. Rotor current i_{ra} vs time, magenta – linear case, blue – nonlinear case.

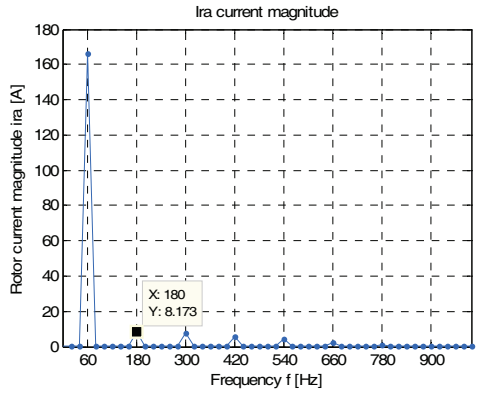

Fig. 23. Rotor current magnitude I_{ra} vs. frequency.

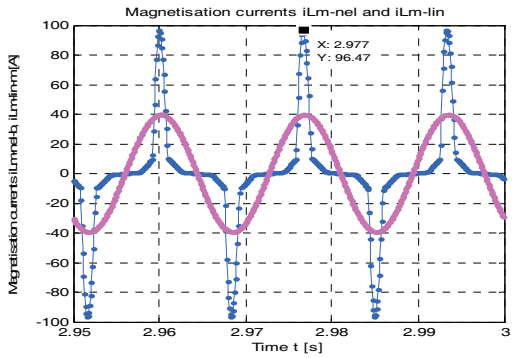

Fig. 24. Magnetization current i_{Lm} vs time.

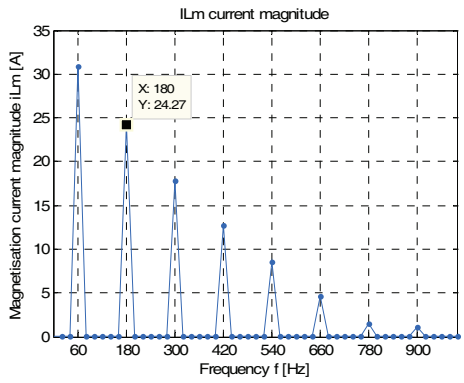

Fig. 25. Magnetization current magnitude I_{Lm} vs. frequency.

The time variation of the stator current i_{sA}, for the nonlinear (saturated) magnetic circuit, shows a very close shape to the one obtained when the magnetic circuit is linear (non-saturated). This coincidence relies on the very small variations of the magnetization inductance in comparison to the variations of the rotor parameters from the equivalent circuit (Fig. 19).

The high order harmonic magnitudes of the stator current are relatively small comparing to the fundamental magnitude (Fig. 21), because the waveform of the stator current is approximately sinusoidal. Consequently the Joule losses produced by these harmonics are small (less than 1% than those produced by the fundamental).The same remarks can be made about the rotor current i_{ra} (Fig. 22 and 23).

The magnetization current i_{Lm} (Fig. 24) displays a strong distortion, due to the strong saturation assumed in this study and the current magnitude is about double comparing with the linear case. Therefore the high order harmonic magnitudes are important.

The voltage across the inductor v_{Ls}, being proportional to the derivative of the current i_{sA}, $v_{Ls} = L_s \frac{\mathrm{d}i_{sA}}{\mathrm{d}t}$, is more distorted than the current. The weight of the third order harmonic of i_{sA} and of v_{Ls} with respect to the fundamental is:

$$\varepsilon_{i_{sA}} = \frac{19.34}{175} \cdot 100 = 11\%,$$

respectively

$$\varepsilon_{v_{Ls}} = \frac{23.51}{70} \cdot 100 = 33.58\% .$$

V. Conclusions

This paper presents a method of assembling a mathematical model for squirrel cage induction machine with deep rotor bars considering the influence of skin effect on the electrical parameters of the rotor. The model developed here gives the possibility to perform studies regarding the steady state and dynamic behavior of the induction motor with deep bars in the rotor and to assess its performances.

The frequency of stator currents is considered constant, equal to the network frequency.

In fact, even the rotor parameters are considered constant, independent of the rotor frequency, in conditions of low rotor frequency values (0 and 10...15) Hz. For higher rotor frequencies the authors proposed for the rotor resis-

tance and the rotor leakage inductance analytic expressions of angular rotor frequency, resulting from the skin effect theory. For the dynamic (transient) behavior analysis purposes we've used a state model derived from the Park-Blundell equations. These equations have a nonlinear form due to: their structure, frequency variation of the rotor parameters, saturation phenomena, and the variation of the load torque with respect to the rotor angular frequency. The integration of these equations is performed with the help of the integration routines developed for ordinary differential equations and available in MATLAB programming environment. The steady state behavior analysis of the deep bars induction motor requires the use of the ∏ (Steinmetz) equivalent scheme of the induction motor, where the magnetization inductance is considered as the current-controlled nonlinear inductor and the rotor resistance as a time-variable resistor. The simulations were done by ENCAP – Electrical Nonlinear Circuit Analysis, and, for the reason of results comparison by the SPICE program. Both of these programs are based upon the modified nodal equations and they allow the Fourier analysis for all current and voltage waveforms. In this way we can compute the magnitude of each, arbitrarily chosen harmonic from the voltage/current waveform. Analyzing the obtained results we conclude that due the high order harmonic in the current waveforms the losses increase worsening the induction motor performances (as: the efficiency, power factor etc). When comparing the nominal values obtained through simulations with the catalog data, we found out a very good agreement.

REFERENCES

[1] A. K. Repo, P. Rasilo, and A. Arkkio, "Dynamic electromagnetic torque model and parameter estimation for a deep-bar induction machine", *IET Electr. Power Appl*., vol. 2, No. 3, pp. 183 -192, 2008.

[2] E. Levi, "Main flux saturation modelling in double-cage and deep-bar induction machines", *IEEE Trans. Energy Conversion*, vol. 11, No. 2, pp.305 – 311, 1996.

[3] K. S. Huang, Q.H. Wu, and D.R. Turner, "Effective identification of induction motor parameters based on fewer measurements", *IEEE Trans. Energy Converssion*, vol. 17, No. 1, pp.305 – 311, pp. 55 – 59, 2002.

[4] D. J. Atkinson, J. W. Finch, and P. P. Acarnley, "Estimation of rotor resistance in induction motors", *IEE Proc. Electr. Power Appl.*, vol. 143, no.1, pp. 87 -94, 1996.

[5] J. Pedra, L. Sainz, "Parameter estimation of squirrel-cage induction motors without torque measurements", *IEE Proc. Electr. Power Appl*., vol. 153, no.2, pp. 87 -94, 2006.

[6] W. A. A. Rik, De Doncker, "Field-Oriented Controllers with Rotor Deep Bar Compensation Circuits", *IEEE Trans. Industry Applications*, vol. 28, nr. 5, pp. 1062 – 1070, 1992.

[7] N. Galan, *Electrical Machines*, Roumanian Academic Publishing, Bucharest, 2011.

[8] J. K. Seok, and S. K. Sul, "Pseudorotor-flux-oriented control of an induction machine for deep-bar-effect compensation", *IEEE Trans. Industry Applications*, vol. 34, nr. 3 , pp. 429 – 434 , 1998.

[9] C. Alexander, C. Smith, C. Russell, C. Healez, and W. Stephen, "A transient induction motor model including saturation and deep bar effect", *IEEE Trans. Energy Converssion*, vol. 11, No. 1, pp.8 -15, 1996.

[10] M. Iordache, Lucia Dumitriu, and I. Matei, *ENCAP – Electrical Nonlinear Circuit Analysis Program*, User Guide, Department Electrical Library, Politehnica University of Bucharest, 2001.

[11] M. Iordache, Lucia Dumitriu, *SYMNAP – SYmbolic Modified Nodal Analysis*, User Guide, Library of Electrical Department, PUB, Bucharest, 2000.

[12] C. Mihăilrscu, Fl. Rezmeriță, Ileana Calomfirescu, M. Iordache, and N. Galan, "Performance analysis of three phase-squirred cage induction motor with deep rotor bars in transient behavior", *Electrical and Electronic Engineering*, p-ISSN:2162-9455 e-ISSN: 2162-8459, vol. 2, No. 2, 2012, pp. 11-17.

[13] A. Câmpeanu, *Introduction in Dynamic of Electrical Machines in Alternating Current* (*Introducere în Dinamica Maşinilor Electrice de Curent Alternativ*), Editura Academiei, Bucureşti, 1998.

[14] M. Iordache, Lucia Dumitriu, N. Galan, D. Niculae, and Ileana Calomfirescu, "Saturation influence on induction motor working in steady-state behavior", *ACTA Electrotehnica*, Special Issue, Proceedings of the 5nd International Conference on Modern Power Systems MPS 2013 28-31 of May 2013, Cluj-Napoca, Romania, Mediamira Science Publisher, pp. 229 – 232.

[15] S. Deleanu, *Contributions on the AC Electrical Drives Used in Traction* (*Contribuţii privind acţionările electrice de curent alternativ utilizate in tracţiune*), PhD Thesis, "Politehnica" University of Bucharest, 2001.